UNIVERSITY OF CALIFORNIA
RIVERSIDE

Analysis of the Multidimensional Effects in Biofilms

A Thesis submitted in partial satisfaction
of the requirements for the degree of

Master of Science

in

Mechanical Engineering

by

Michael Benjamin Hauser

June 2012

Thesis Committee:

Dr. Kambiz Vafai, Chairperson
Dr. Charles Wyman
Dr. Marko Princevac

The Thesis of Michael Benjamin Hauser is approved:

_____

_____

_____

Committee Chairperson

University of California, Riverside

ACKNOWLEDGEMENTS

Thank you to my parents, brothers, sister, family, friends, students and colleagues. I would specifically like to thank my lab mates and class mates Ana Quezada, พรรณไท คำแดงยอดไตย, Shujuan Wang, Shirin Mesbah, Maryam Shafahi, Uzair Ahmed, Arman Haghighi, Hayden Dahl, Karim Alizad, Stephen Chung, Monzur Morshed, William Bailey and Anthony Fong for helping me with my thesis and other school work at UCR. I would like to thank the UCR Mechanical Engineering administrative staff of Roseanna Barron, Katie Dell, Sarah Nosce and Paul Talevera for answering my many questions. I would like to thank the University of California for generously supporting my graduate studies through the Dean's Distinguished Fellowship as well as numerous teaching positions. I would like to thank my undergraduate advisors Prof. Henry van Driel and Prof. Charles Dyer from the University of Toronto for their initial and continuing support of my budding scientific career.

I would like to thank my committee members Prof. Charles Wyman, Prof. Marko Princevac and Prof. Kambiz Vafai, each of whom have taught me a great deal about the similarities and differences of science and engineering, and how to excel in each of those fields. Finally, I would like to thank again my advisor Prof. Kamibz Vafai, who has been a truly exceptional mentor, teaching me how to produce both publishable and meaningful scientific work, always stressing the latter even if many others pursue the former.

DEDICATION

This document is dedicated to my family and friends.

ABSTRACT OF THE THESIS

Analysis of the Multidimensional Effects in Biofilms

by

Michael Benjamin Hauser

Master of Science, Graduate Program in Mechanical Engineering
University of California, Riverside, June 2012
Dr. Kamibz Vafai, Chairperson

A general multidimensional, multispecies, heterogeneous biofilm model is developed using the balance equations. Multidimensional effects are studied by taking limiting scenarios towards lower dimensional analogues, as well as studying the effects of changing biofilm surface geometries. Error-maps are developed suggesting when single-dimensional models give an accurate representation of biofilm growth, and when multidimensional effects are substantial. A porous media model is studied, where the bacteria *Pseudomonas aeruginosa* is modeled to grow in a packed porous bed of spheres. It is found that under most circumstances, single-dimensional models predict very similar growth rates as compared to their multidimensional analogues. However, under some conditions, the multidimensionality can have a significant effect in the model's predictions. To the authors' best knowledge, this is the first work which develops error maps detailing multidimensional effects of biofilm growth.

TABLE OF CONTENTS

LIST OF FIGURES

Figure

CHAPTER 1

Introduction

1.1 Definition and Formation of Biofilm

Biofilms are communities of bacterial cells that are adherent to surfaces and are protected by a self-created extracellular polymeric substance (EPS). Free floating, planktonic bacteria can exhibit very different traits when compared to the same species of bacteria inhabiting a biofilm.

Biofilm research has far reaching implications and applications. Biofilm research has proven valuable in fields as diverse as medicine, where it has been used in the development of antibiotic medication [1], as well as the study of biofilm growth on implanted devices after surgery [2], or to wastewater management [3], in which biofilms are introduced into the system to digest and remove harmful organic or inorganic compounds from wastewater.

In order for a biofilm to develop, a bacterial cell must adhere to a surface. From this point, other planktonic cells may attach to this initial cell, or instead they may also attach to the substratum. The attached bacteria then grow and divide, increasing the communal population of the biofilm. The bacteria also produce their protective EPS at stoichiometric rates, which help increase the livelihood of the entire biofilm community. The bacteria will die if there is a lack of available nutrients in their environment. Through the use of quorum sensing, the bacteria can communicate their population and coordinate activation of various traits [4].

1.2 Biofilm modeling

It is common for different species of bacteria to live together and compete for nutrients and space, thus multispecies and multisubstrate effects are important attributes to include in the development of comprehensive biofilm models. There exists a diverse set of methods used to model these interactions, with the most popular being to model the biofilm using continuum mechanics [5] [6] [7] [8] [9], individual-based models [10] [11] [12], cellular automaton [13] [14], and combinations there-of [15] [16].

Biofilm models developed from continuum mechanics assume the biofilm to vary continuously in space and time. These models are based on principle results of continuum mechanics such as Reynold's Transport Theorem and Fick's Law, with biofilm growth and death behaving as sources and sinks in a velocity field of biofilm expansion and compression. This is an attractive framework for biofilm modeling because it is based on nearly 200 years of well-established theory, and this is the model form that this research uses.

Individual-based models are rather different in that they model the dynamics of the individual bacteria composing the biofilm. An individual bacterial cell is usually represented as a simple geometric object such as a sphere, which gets larger as nutrients are consumed. Eventually the cell grows large enough such that at a certain critical radius the sphere splits into two spheres, which is analogous to cell division. When spheres overlap, rules exist which suggest how they should push each other apart, which on a macroscopic level results in biofilm expansion. The strength of this framework is that it provides a means to model individual cellular interactions.

Biofilm models based on cellular-automata are interesting because, by construction they have the ability to model bacterial interactions which occur on a local level in a natural way. They do this through sets of rules for nutrient consumption, growth, expansion, and properties of neighboring cells, which ultimately results in a global picture of biofilm dynamics. The framework of cellular automaton is particularly well suited for modeling bacteria on a local level because through basic, well-formed sets of rules one is able to represent a wide array of complex interactions, which can be difficult to formulate using differential equations.

Earlier work in biofilm modeling led to fairly simple yet powerful one dimensional continuum models, with one dimensional growth occurring orthogonal to the substratum [5] [17] [18]. One dimensional continuum models can have the ability to capture important effects, such as species competition for space and nutrients, which leads to a globally heterogenous biofilm structure [5]. Biofilm heterogeneity is a result of different species having different nutrient uptake rates, different growth rates and different EPS production rates. Heterogeneity in nutrient concentration is also captured in these one dimensional models, in part since different nutrients have different diffusion rates as well as different consumption rates. These are very important effects, which can be captured in one dimension.

Drawbacks to one dimensional models are that, for some cases which constitute a smaller subset of available scenarios, spatial heterogeneities do not necessarily occur only in the direction orthogonal to the substratum, but instead growth and diffusion processes can also occur parallel to that plane. If a spatial gradient exists in the nutrient concentration in the horizontal direction, then one would have a horizontal component of the nutrient

flux. This would also result in bacterial species growing along this gradient, leading to a heterogeneous distribution of bacterial species in the horizontal direction within the biofilm. The impact of these types of growths needs to be assessed.

For example, in nutrient limited regimes and under conditions with sufficiently large mass transfer boundary layers biofilm fingering formation can occur [6] [7], which is a multidimensional effect. This complex surface geometry affects nutrient diffusion processes, which itself affects species growth rates. By using one-dimensional models one is ignoring the effects of the surface geometry.

A second example of a multidimensional system is seen in a partially mixed multispecies system. One would expect to see spatial heterogeneities of bacterial species in the vertical as well as horizontal directions, and considering different bacterial species have different growth and consumption properties, these heterogeneities can lead to multidimensional species competition [6] [10].

1.3 Structure of Thesis

It is the purpose of this work to study these multidimensional characteristics, their absolute influences on net growth rate, and finally to develop error mappings which can be used to suggest when multidimensional characteristics are necessary for accurate prediction of biofilm growth. In Chapter 2, the general biofilm model based on continuum mechanics is developed. Chapter 3 is devoted to explaining the techniques used to numerically solve these sets of equations. Chapter 4 gives the 2 specific biofilm models which are studied in this research, the first being a 3-species toy model composed of heterotrophic bacteria, autotrophic bacteria, and EPS, and the second being a 2-species

model composed of *Pseudomonas aeruginosa* and EPS. Chapter 5 develops error mappings between the 1, 2 and 3 dimensional 3-species models by taking limiting scenarios of higher dimensional models towards lower dimensional analogues. At the end of Chapter 5 comparisons are made between 1, 2 and 3 dimensional biofilm growth of the 2-species model, and applies these models to a porous bed modeled as a heterogeneous packed bed of spheres.

CHAPTER 2

General Biofilm Model

As already stated, the analysis is performed using a multidimensional, multispecies, multisubstrate, heterogeneous biofilm model based on constitutive equations from continuum mechanics.

Nomenclature

Dependent Variables		*Constants*	
$\rho_s = \rho_s(x,y,z,t)$	Density of species *s*	ρ_s^*	Density of species *s*
$v_s = v_s(x,y,z,t)$	Volume fraction of species *s*	D_n	Constant scalar diffusion coefficient for nutrient *n*
$C_n = C_n(x,y,z,t)$	Concentration of nutrient *n*	λ	Biomass detachment coefficient
$\vec{S} = (x,y,Z(x,y,t))$	Parametric form of surface	μ_s	Growth rate of species *s*
$\vec{u} = \vec{u}(x,y,z,t)$	Biofilm expansion velocity	K_n^s	Monod saturation constant for species *s* and nutrient *n*
$\Phi = \Phi(x,y,z,t)$	Biofilm expansion potential	b_s	Endogenous rate constant for species *s*
		k_s	Inactivation rate constant for species *s*
Reaction Rates		Y_s	Biomass yield for species *s*
$g_s = g_s(x,y,z,t)$	Growth rate for species *s*	α_s	Conversion factor for species *s*
$r_n = r_n(x,y,z,t)$	Reaction rate for nutrient *n*	C_{nB}	Bulk fluid concentration for nutrient *n*
		i	Stoichiometric factor - EPS/*Pa*
		k	Stoichiometric factor - Gl/O_2
Scaling Factors		*Dimensionless variables*	
L_x	Domain width in x-direction	x'	Dimensionless x-variable
L_y	Domain width in y-direction	y'	Dimensionless y-variable
$Z = Z(x,y,t)$	Functional form of surface	z'	Dimensionless z-variable
τ	Characteristic time scale	t'	Dimensionless time-variable

Figure 1-Nomenclature

2.1 Derivation of Governing Equations

The derivations of the governing equations have been influenced by previous work [5] [6] [8]. The biofilm is assumed to live in three spatial dimensions and one temporal dimension, i.e. $\mathbb{R}^3 \otimes \mathbb{R}$.

The biofilm is assumed to have continuous properties and growth will follow the continuity equation. Biofilm expansion is convection dominated, so for bacterial species *s*:

$$\frac{\partial \rho_s}{\partial t} + \vec{\nabla} \cdot \left(\vec{u} \rho_s \right) = g_s \tag{1}$$

The dependent variables are defined such that ρ_s is the density of species *s*, g_s is the growth rate of species *s*, and $\vec{u}$ is the biofilm expansion velocity. If it is assumed that the density of species *s* across the biofilm domain is constant $\rho_s^* \in \mathbb{R}$, then $\rho_s = \rho_s^* v_s$, where v_s is the dependent function for volume fraction of species *s* in the biofilm. The biofilm growth equation becomes:

$$\frac{\partial v_s}{\partial t} + \vec{\nabla} \cdot \left(\vec{u} v_s \right) = \frac{g_s}{\rho_s^*} \tag{2}$$

Using the fact that $\sum_s v_s = 1$, one finds:

$$\vec{\nabla} \cdot \vec{u} = \sum_s \frac{g_s}{\rho_s^*}. \tag{3}$$

The growth equations can then be simplified to:

$$\frac{\partial v_s}{\partial t} + \vec{u} \cdot \vec{\nabla} v_s = \frac{g_s}{\rho_s^*} - v_s \sum_i \frac{g_i}{\rho_i^*} \tag{4}$$

Nutrient concentration for nutrient *n* within the biofilm is diffusion dominated and can be presented as:

$$\frac{\partial C_n}{\partial t} = D_n \nabla^2 C_n + r_n \tag{5}$$

where the dependent variables are defined such that C_n is the nutrient concentration for nutrient *n* and r_n is the reaction rate.

Because diffusion processes occur much faster than biofilm growth processes, and we are interested in biofilm growth processes, one may assume that the nutrient concentration has reached steady state over biofilm growth process time scales [19].

$$D_n \nabla^2 C_n + r_n = 0 \tag{6}$$

An order of magnitude argument can be made to justify this approximation. Diffusion coefficients of nutrients within biofilm are of order $D \sim 100 \cdot 10^{-6} \mathrm{m}^2 / \mathrm{days}$ while lengths scales of biofilm are of order $l \sim 10^{-3} \mathrm{m}$, which imply that nutrient diffusion velocities within biofilm are of order $v_D \sim D / l \sim 10^{-1} \mathrm{m} / \mathrm{days}$. Furthermore, biofilm grow to length scales of order $l \sim 10^{-3} \mathrm{m}$ in $t \sim 10 \mathrm{days}$, which implies that biofilm growth velocities are of order $v_G \sim l / t \sim 10^{-4} \mathrm{m} / \mathrm{days}$. Thus diffusion velocities are 3 orders of magnitude greater than growth velocities, implying that the steady state approximation of nutrient diffusion is valid.

The parametric form of the biofilm surface $\vec{S}(x,y,t) = \left(x, y, Z(x,y,t)\right)$ is related to the expansion velocity as follows:

$$\frac{\partial \vec{S}}{\partial t} = \vec{u}\,|_{z=Z} \tag{7}$$

The integral form of this differential equation is:

$$\vec{S} = \vec{S}_o + \int_0^t \vec{u} dt \tag{8}$$

One way in which shearing forces can be incorporated into the model is by modifying the differential equation for the biofilm surface [5]:

$$\frac{\partial \vec{S}}{\partial t} = \vec{u}\,|_{z=Z} - \lambda Z^2 \hat{z} \tag{9}$$

where λ is a constant specifying the relative strength of shearing forces.

2.2 Governing Equations in Potential Formulation

The governing equations can be simplified by assuming irrotational growth [6] [7]. The expansion velocity may then be taken as the negative gradient of a scalar potential $\vec{u} = -\vec{\nabla}\Phi$. The governing equations in the final, coordinate-free form can be presented as:

$$\frac{\partial v_s}{\partial t} - \vec{\nabla}\Phi \cdot \vec{\nabla} v_s = \frac{g_s}{\rho_s^*} - v_s \sum_i \frac{g_i}{\rho_i^*} \tag{10}$$

$$D_n \nabla^2 C_n + r_n = 0 \tag{11}$$

$$\nabla^2\Phi = -\sum_i \frac{g_i}{r_i^*} \tag{12}$$

$$\vec{S} = \vec{S}_o - \int_0^t \vec{\nabla}\Phi dt \tag{13}$$

For all of the equations, the boundary conditions are assumed to be periodic in the horizontal directions and no-flux at the substratum. For the nutrient equations, a constant bulk fluid nutrient concentration is taken at the surface of the biofilm. For the potential equation, because of the gauge freedom associated with defining a potential, we define the potential at the biofilm surface to be zero.

CHAPTER 3

Analysis and Solution Methodology

3.1 Numerical Difficulties Associated with Biofilm Modeling

One of the major difficulties associated with multidimensional biofilm modeling is tracking the moving boundary and defining a boundary condition on this dynamically changing boundary. The method used here is to solve the sets of equations in a specifically chosen curvilinear coordinate space, chosen such that the generally varying biofilm surface boundary will be constant in the new coordinate space. Thus some of the difficulties associated with defining a boundary condition on the oddly shaped, dynamically moving biofilm surface will not pose problematic. A second method often employed for tracking the moving boundary is by solving the equations within a level-set framework [6] [7] [20].

A significant advantage to defining the boundary conditions in this new coordinate space is that one is able to study biofilm growth over large changes in length scales. This is clearly appropriate to biofilm modeling because biofilm start as individual bacteria, which have length scales on the order of micrometers, and they can grow to become entire biofilm communities, which have length scales on the order of millimeters, which is a change of three orders of magnitude. A disadvantage of using this solution method is that since one is working in a curvilinear coordinate system, three-dimensional simulations can take much longer to finish. After the calculations are done in the curvilinear space, one must then convert back to Euclidean space to make physical sense of the results. The derivation of the coordinate transformation is presented in three spatial dimensions, however the two dimensional derivation is completely analogous.

3.2 Derivation of Coordinate Mapping

If L_x and L_y are the widths of the domain, $Z\left(x,y,t\right)$ the biofilm surface, and τ the characteristic time scale, then define the coordinate mapping as follows:

$$x' = \frac{x}{L_x} \tag{14}$$

$$y' = \frac{y}{L_y} \tag{15}$$

$$z' = \frac{z}{Z\left(x,y,t\right)} \tag{16}$$

$$t' = \frac{t}{\tau} \tag{17}$$

Finding the new derivative operators requires knowledge of the Jacobian matrix $\frac{\partial}{\partial x^a} = J_a^b \frac{\partial}{\partial x'^b},\ a,b = 1,2,3,4$. Einstein summation notation is used, where a repeated index implies summation and $\frac{\partial}{\partial x^a} = \partial_a$ is written for brevity. The new derivative operators are:

$$\frac{\partial}{\partial x} = \frac{1}{L_x}\frac{\partial}{\partial x'} - \frac{z'}{L_x}\frac{\partial_{x'}Z}{Z}\frac{\partial}{\partial z'} \tag{18}$$

$$\frac{\partial}{\partial y} = \frac{1}{L_y}\frac{\partial}{\partial y'} - \frac{z'}{L_y}\frac{\partial_{y'}Z}{Z}\frac{\partial}{\partial z'} \tag{19}$$

$$\frac{\partial}{\partial z} = \frac{1}{Z}\frac{\partial}{\partial z'} \tag{20}$$

$$\frac{\partial}{\partial t} = \frac{1}{\tau}\frac{\partial}{\partial t'} - \frac{z'}{\tau}\frac{\partial_{t'}Z}{Z}\frac{\partial}{\partial z'} \tag{21}$$

In the new coordinate space, the Laplacian operator becomes:

$$\nabla^2 = \left(\frac{1}{L_x}\frac{\partial}{\partial x'} - \frac{z'}{L_x}\frac{\partial_{x'}Z}{Z}\frac{\partial}{\partial z'}\right)^2 + \left(\frac{1}{L_y}\frac{\partial}{\partial y'} - \frac{z'}{L_y}\frac{\partial_{y'}Z}{Z}\frac{\partial}{\partial z'}\right)^2 + \left(\frac{1}{Z}\frac{\partial}{\partial z'}\right)^2 \tag{22}$$

This expands to the following:

$$\nabla^2 = \frac{1}{{L_x}^2}\frac{\partial^2}{\partial x'^2} + \frac{1}{{L_y}^2}\frac{\partial^2}{\partial y'^2} + \frac{1}{Z^2}\left(1 + z'\left(\left(\frac{\partial_{x'}Z}{L_x}\right)^2 + \left(\frac{\partial_{y'}Z}{L_y}\right)^2\right)\right)\frac{\partial^2}{\partial z'^2} - 2\frac{z'}{{L_x}^2}\frac{\partial_{x'}Z}{Z}\frac{\partial^2}{\partial x'\partial z'}$$
$$-2\frac{z'}{{L_y}^2}\frac{\partial_{y'}Z}{Z}\frac{\partial^2}{\partial y'\partial z'} + \frac{z'}{Z^2}\left(\frac{2\left(\partial_{x'}Z\right)^2 - \left(\partial_{x'^2}Z\right)Z}{{L_x}^2} + \frac{2\left(\partial_{y'}Z\right)^2 - \left(\partial_{y'^2}Z\right)Z}{{L_y}^2}\right)\frac{\partial}{\partial z'} \tag{23}$$

3.3 Formulation of Governing Equations in the new Coordinate Space

With the derivative operators defining the new vector space, the initial and boundary conditions may be set. Note that for brevity the Neumann conditions are defined in terms of the Euclidean derivative operators instead of the derivative operators found to describe the new space.

$$\frac{\partial v_s}{\partial t} - \vec{\nabla}\Phi \cdot \vec{\nabla} v_s = \frac{g_s}{\rho_s^*} - v_s \sum_i \frac{g_i}{\rho_i^*}$$

I.C. $v_s\left(x', y', z', 0\right) = v_{s0}\left(x', y', z'\right)$

B.C. $v_s\left(0, y', z', t'\right) = v_s\left(1, y', z', t'\right),$

$v_s\left(x', 0, z', t'\right) = v_s\left(x', 1, z', t'\right),$

$\frac{\partial v_s}{\partial z}\left(x', y', 0, t\right) = 0$ (24)

$$D_n \nabla^2 C_n + r_n = 0$$

B.C. $C_n\left(0, y', z', t'\right) = C_n\left(1, y', z', t'\right),\ \frac{\partial C_n}{\partial x}\left(0, y', z', t'\right) = \frac{\partial C_n}{\partial x}\left(1, y', z', t'\right)$

$C_n\left(x', 0, z', t'\right) = C_n\left(x', 1, z', t'\right),\ \frac{\partial C_n}{\partial y}\left(x', 0, z', t'\right) = \frac{\partial C_n}{\partial y}\left(x', 1, z', t'\right)$

$C_n\left(x', y', 1, t'\right) = C_{nB},\ \frac{\partial C_n}{\partial z}\left(x', y', 0, t'\right) = 0$ (25)

$$\nabla^2 \Phi = -\sum_i \frac{g_i}{r_i^*}$$

B.C. $\Phi\left(0, y', z', t'\right) = \Phi\left(1, y', z', t'\right),\ \frac{\partial \Phi}{\partial x}\left(0, y', z', t'\right) = \frac{\partial \Phi}{\partial x}\left(1, y', z', t'\right)$

$\Phi\left(x', 0, z', t'\right) = \Phi\left(x', 1, z', t'\right),\ \frac{\partial \Phi}{\partial y}\left(x', 0, z', t'\right) = \frac{\partial \Phi}{\partial y}\left(x', 1, z', t'\right)$

$\Phi\left(x', y', 1, t'\right) = 0,\ \frac{\partial \Phi}{\partial z}\left(x', y', 0, t'\right) = 0$ (26)

$$\vec{S} = \vec{S}_o - \int_0^t \vec{\nabla}\Phi dt$$

I.C. $\vec{S}_0 = \left(x, y, Z\left(x, y, z, 0\right)\right)$ (27)

3.4 Numerical Solution Methods

The covariant transformation maps the irregularly shaped biofilm domain onto a square domain in a curvilinear coordinate space. Fourth order accurate finite differencing

approximations were applied to these sets of equations on a uniform fixed grid and programmed in *Mathematica*. By using 20 nodes in each direction, an error term of less than 0.01% is attained. Derivations of the specific finite difference equations used are given in Appendix A. The first step of the computational scheme was to initialize the surface of the biofilm and volume fractions of the biofilm species. Subsequent steps were to iteratively calculate in time the changing surface, volume fractions, nutrient concentrations and potential. The surface and volume fraction equations were solved explicitly, while the nutrient and potential equations were solved implicitly. A schematic of the computational scheme is provided in Fig. 2. Simulations were run on a PC with an Intel Core i7 processor. Two dimensional simulations took up to 5 minutes to finish, while three dimensional simulations took up to 40 hours to finish.

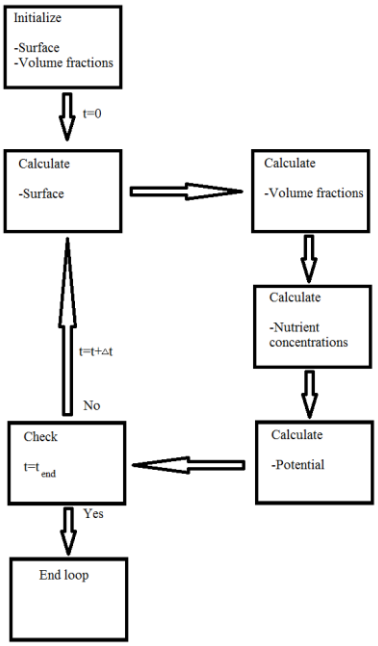

Figure 2-Computational Scheme

CHAPTER 4

Biofilm Model

4.1 Three species Biofilm model

Solutions were found for a representative biofilm model composed of Heterotrophic bacteria, Autotrophic bacteria and EPS [5] [6]. Heterotrophic and Autotrophic species consume Glucose and Ammonium, respectively, and they both consume Oxygen. The biofilm growth kinetics are described by monod expressions. For brevity, Heterotrophic, Autotrophic and inert species are denoted by 1, 2 and 3, respectively, and Glucose, Ammonium and Oxygen, are denoted by 1, 2 and 3, respectively. Parameter constants can be found in Wanner-Gujer [5].

$$g_1 = \mu_1 \rho_1^* v_1 \frac{C_1}{K_1^1 + C_1} \frac{C_3}{K_3^1 + C_3} - b_1 \rho_1^* v_1 \frac{C_3}{K_3^1 + C_3} - k_1 \rho_1^* v_1 \tag{28}$$

$$g_2 = \mu_2 \rho_2^* v_2 \frac{C_2}{K_2^2 + C_2} \frac{C_3}{K_3^2 + C_3} - b_2 \rho_2^* v_2 \frac{C_3}{K_3^2 + C_3} - k_2 \rho_2^* v_2 \tag{29}$$

$$g_3 = k_1 \rho_1^* v_1 + k_2 \rho_2^* v_2 \tag{30}$$

Nutrient consumption by the biofilm directly affects the nutrient concentration:

$$r_1 = -\frac{1}{Y_1} \mu_1 \rho_1^* v_1 \frac{C_3}{K_3^1 + C_3} \frac{C_1}{K_1^1 + C_1} \tag{31}$$

$$r_2 = -\frac{1}{Y_2} \mu_2 \rho_2^* v_2 \frac{C_3}{K_3^2 + C_3} \frac{C_2}{K_2^2 + C_2} \tag{32}$$

$$r_3 = -\frac{\alpha_1 - Y_1}{Y_1}\mu_1\rho_1^*\nu_1\frac{C_3}{K_3^1 + C_3}\frac{C_1}{K_2^1 + C_1} - b_1\rho_1^*\nu_1\frac{C_3}{K_3^1 + C_3}$$
$$-\frac{\alpha_2 - Y_2}{Y_2}\mu_2\rho_2^*\nu_2\frac{C_3}{K_3^2 + C_3}\frac{C_2}{K_2^2 + C_2} - b_2\rho_2^*\nu_2\frac{C_3}{K_3^2 + C_3} \quad (33)$$

4.2 Two speciesBiofilm model

A multidimensional continuum biofilm model is used to study changing permeability of a packed porous bed of spheres. The biofilm is assumed to be composed of the bacterial species *Pseudomonas aeruginosa* and EPS. Growth and diffusion kinetics are described by monod expressions for Glucose and Oxygen, stoichiometric ratios of *Pa* to EPS and Glucose to Oxygen, and yield coefficients. Parameter constants can be found in Wanner-Cunningham-Lundman [21].

$$g_{Pa} = \mu\rho_{Pa}^*\nu_{Pa}\frac{C_{Gl}}{K_{Gl} + C_{Gl}}\frac{C_{O_2}}{K_{O_2} + C_{O_2}} \quad (34)$$

$$g_{EPS} = kg_{Pa} = k\mu\rho_{Pa}^*\nu_{Pa}\frac{C_{Gl}}{K_{Gl} + C_{Gl}}\frac{C_{O_2}}{K_{O_2} + C_{O_2}} \quad (35)$$

Nutrient consumption by the biofilm directly effects the nutrient concentration:

$$r_{Gl} = -\left(\frac{1}{Y_{Pa/Gl}} + \frac{k}{Y_{EPS/Gl}}\right)g_{Pa} = -\left(\frac{1}{Y_{Pa/Gl}} + \frac{k}{Y_{EPS/Gl}}\right)\mu\rho_{Pa}^*\nu_{Pa}\frac{C_{Gl}}{K_{Gl} + C_{Gl}}\frac{C_{O_2}}{K_{O_2} + C_{O_2}} \quad (36)$$

$$r_{O_2} = \frac{1}{i}r_{Gl} = -\frac{1}{i}\left(\frac{1}{Y_{Pa/Gl}} + \frac{k}{Y_{EPS/Gl}}\right)\mu\rho_{Pa}^*\nu_{Pa}\frac{C_{Gl}}{K_{Gl} + C_{Gl}}\frac{C_{O_2}}{K_{O_2} + C_{O_2}} \quad (37)$$

CHAPTER 5

Results and Discussion

Multidimensional effects are studied by taking limiting scenarios towards lower dimensional analogues. This is done by increasing the size of the domain until it is effectively independent of the dimension. An objective of this work is to establish the limiting conditions which will show when lower dimensional models provide a good approximation to higher dimensional ones. Periodic boundary conditions are used to model part of a large system far from the edges, thus when one increases the size of the computational domain one is essentially decreasing the resolution of the heterogeneities associated with multidimensional effects. When the size of the computational domain increases, the effects of the multidimensional heterogeneities decreases tending towards a one dimensional model.

5.1 Comparison of One Dimensional and Two Dimensional Models

Figure 3 shows that the one dimensional model predicts higher growth rates than the analogous two dimensional model, and that the two dimensional model converges to the one dimensional model for large domain widths. One would expect the larger domain to yield higher growth rates since in a larger domain the potential would increase more uniformly from top to bottom. In a smaller domain where multidimensional effects play a more important role, the potential should change relatively more in the horizontal direction, thus horizontal gradients become more relevant. It is expected that parts of these horizontal gradients to interfere with each other, leading to an overall decrease in the biofilm expansion velocity.

The relative differences between the one dimensional and two dimensional models are shown to increase as the size of the domain decreases, as seen in Fig. 4. Interpolating over the relative differences gives a continuous error map over variable domain sizes from 10mm to 50mm, as shown in Fig. 5.

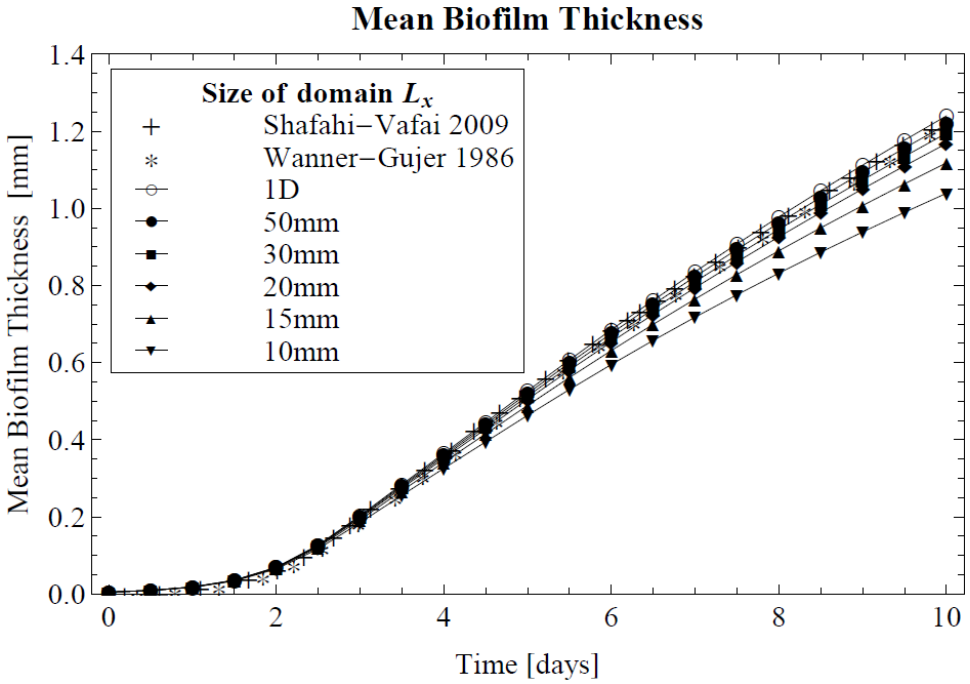

Figure 3-Comparison between 1D and 2D Biofilm Growth with Variable Domain Sizes

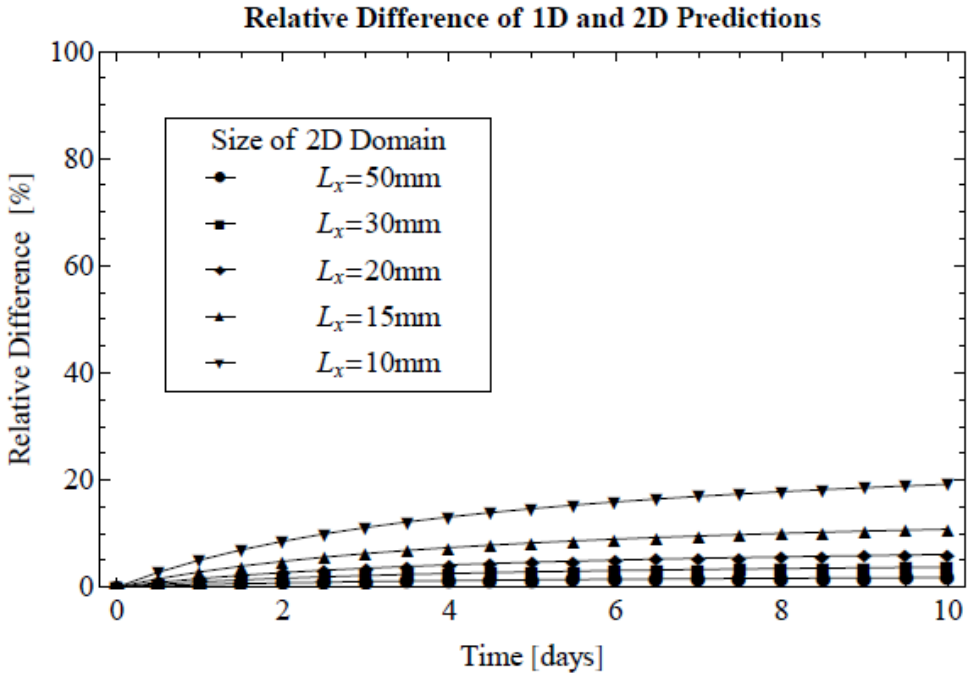

Figure 4-Relative Differences between 1D and 2D Simulations

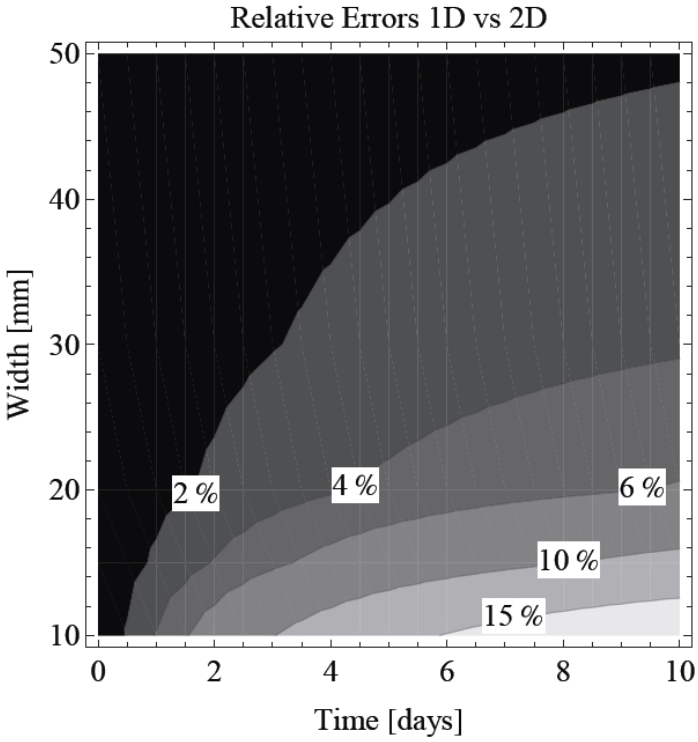

Figure 5-Interpolation of Relative Differences between 1D and 2D Simulations

A change in initial surface geometry results in a change in nutrient diffusion behavior within the biofilm domain which results in a change in biofilm growth. Figure 6 shows the result of changing the relative ratio of surface structure perturbation amplitude to mean initial height, where the perturbation is taken to be a sinusoid on the biofilm surface.

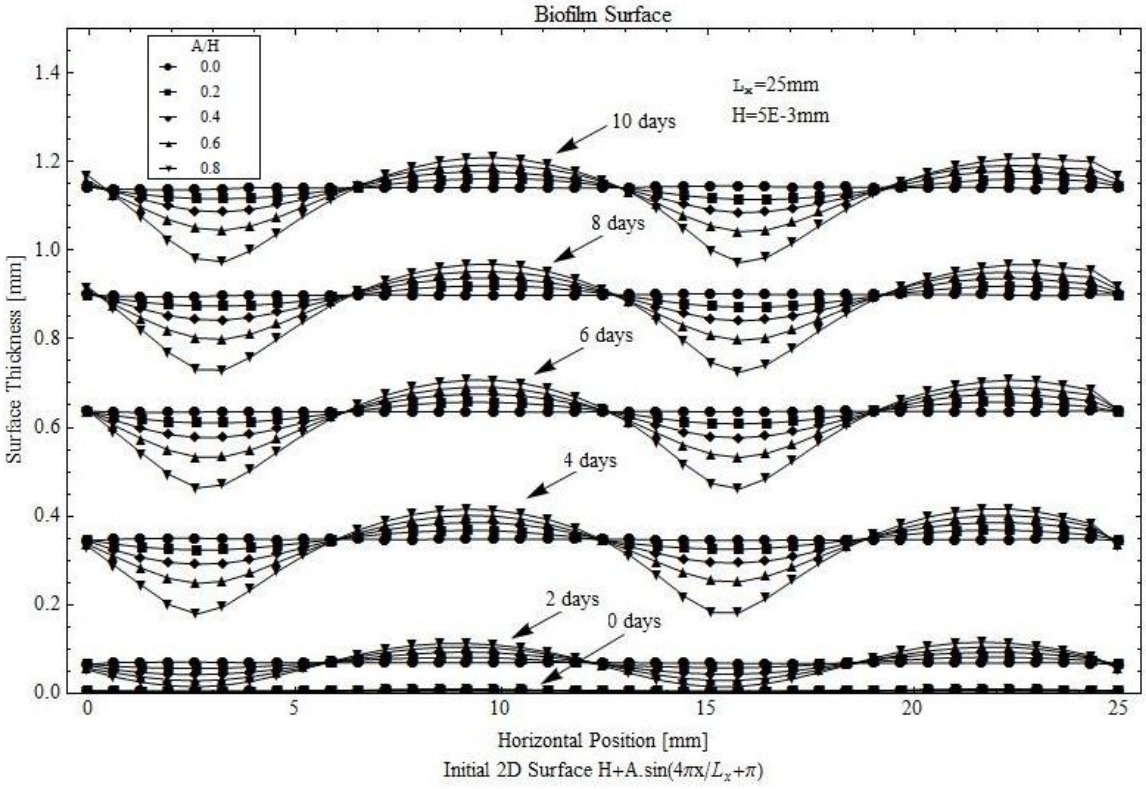

Figure 6-2D Biofilm Growth with Variable Initial Surface Perturbation Amplitude

Upon averaging the biofilm height over the domain, it can be seen that the initial surface geometry plays a minimal role in predicting net biofilm growth, with the net effect averaging out to be similar to a flat surface, as seen in Fig. 7. The case with greater initial surface variations results in slightly slower growth rates, due to the presence of more variations in the horizontal direction at the expense of vertical variations.

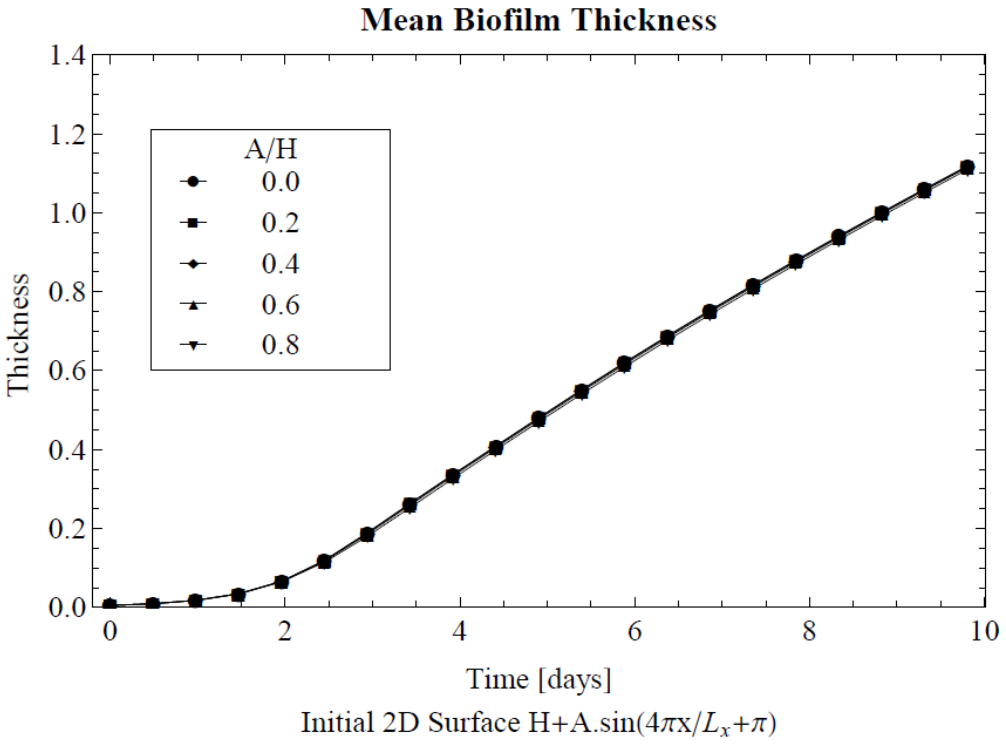

Figure 7-Averaging of 2D Biofilm Growth with Variable Initial Surface Perturbation Amplitude

5.2 Comparison of Two Dimensional and Three Dimensional Models

Figure 8 shows the method used to compare the two dimensional and three dimensional models. Limiting scenarios on the domain were taken such that the domain was shrunk in one direction and held constant in the other, so the shape of the domain is rectangular with a variable aspect ratio. Comparisons were made between the 2D and 3D model predictions. The 2D model effectively matches the 3D model when one domain length is extended beyond a certain limit. Figures 9 and 10 show the effects of changing the size and aspect ratios of the three dimensional domain, and how the three dimensional models converge to their two dimensional analogues at larger domain sizes.

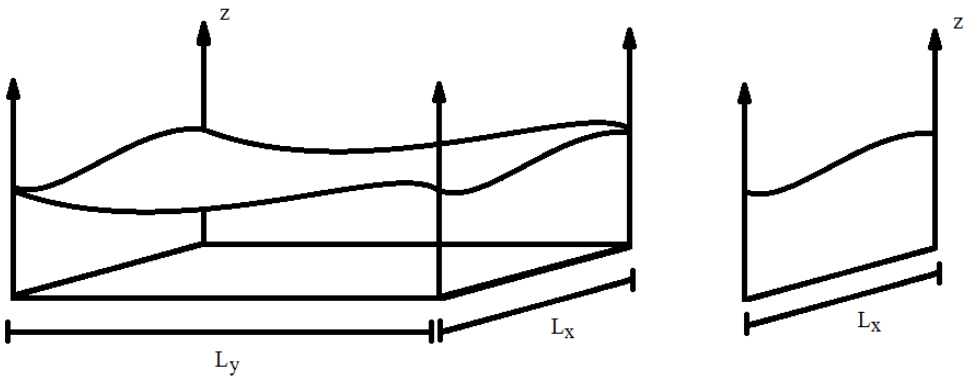

Figure 8-Illustration of 2D and 3D Domain Sizes and Aspect Ratios

The domain in Figure 9a is such that it is held at 50mm in the y-direction while made smaller in the x-direction. As was shown in the two dimensional case, a 50mm domain width provides an excellent approximation of the limiting scenario. Thus the three and two dimensional models predict similar values when one domain width direction is held at 50mm. When the domain is reduced in one direction in Figures 9b, 9c and 9d, due to small widths multidimensional effects become more important in that direction and the two-dimensional model deviates more significantly from the three dimensional growth rate predictions.

As was the case between the 1D and 2D comparisons, the three dimensional biofilm grows more slowly than it does in the equivalent two dimensional case. Again, this is because the potential in the three dimensional case varies more in the horizontal directions than it can in the two dimensional case. Thus the gradient of this potential, which is the biofilm expansion vector, has a larger horizontal component which does not contribute to its vertical growth. Figure 11 displays the error maps establishing the range of validity of 2D model predictions compared to the 3D model. Figure 12 displays the error maps when both the x and y direction lengths are changed at different times.

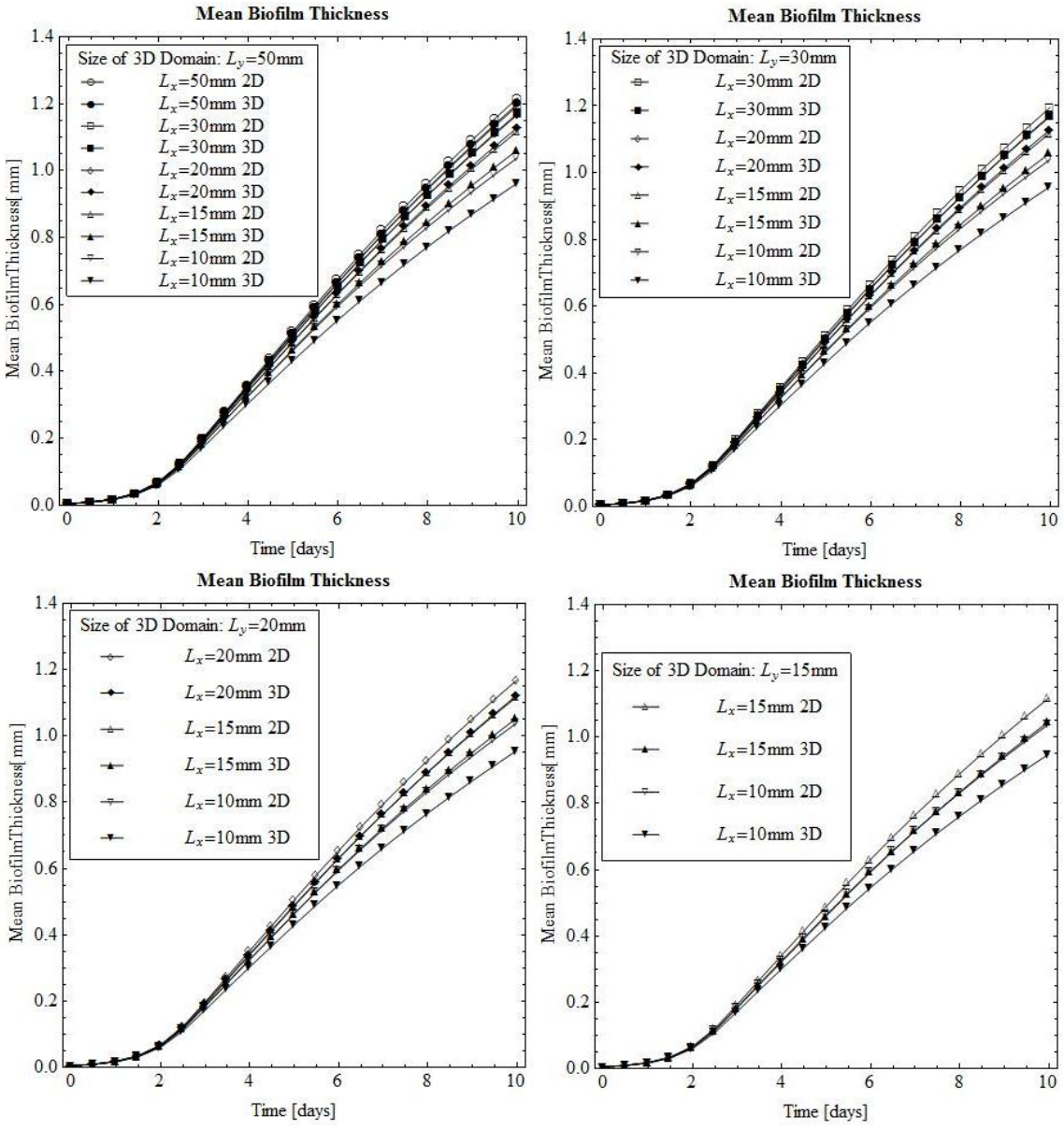

Figure 9-Comparison between 2D and 3D Biofilm Growth with Variable Domain Sizes and Aspect Ratios; a) L_y=50mm, b) L_y=30mm, c) L_y=20mm, d) L_y=15mm

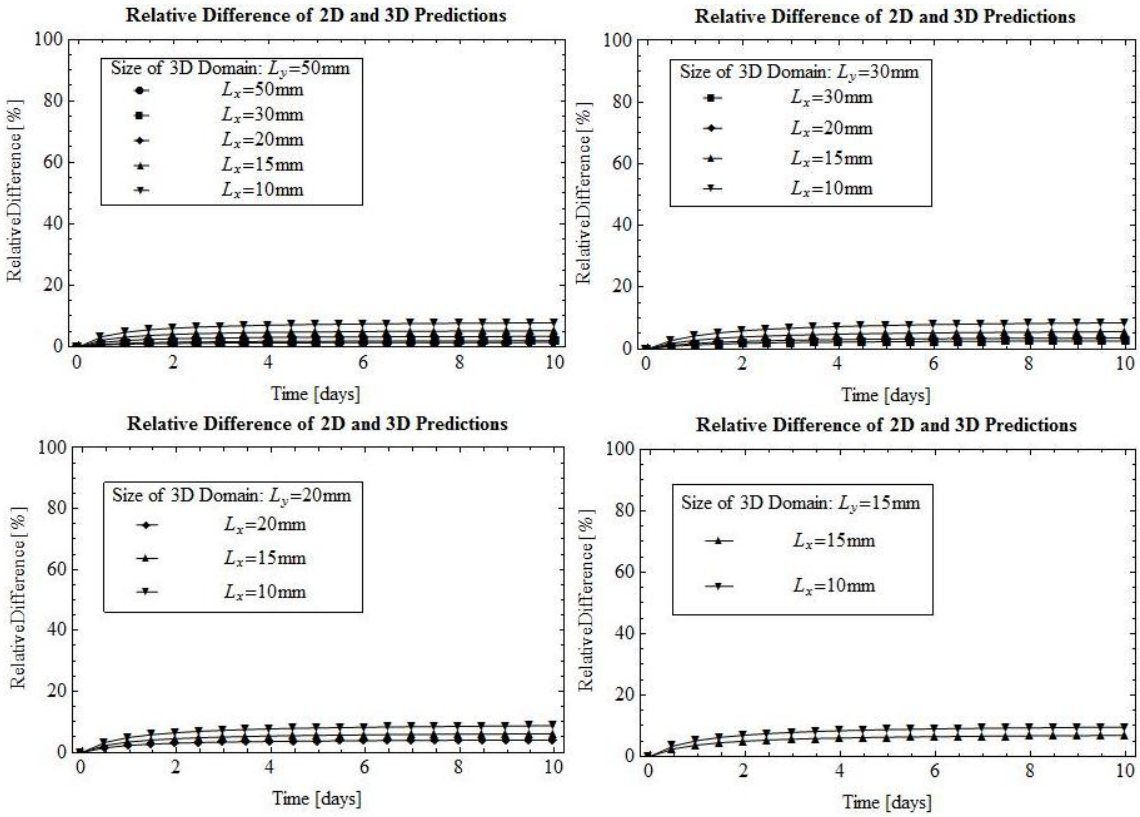

Figure 10-Relative Differences between 2D and 3D Simulations with Variable Domain Sizes and Aspect Ratios; a) L_y=50mm, b) L_y=30mm, c) L_y=20mm, d) L_y=15mm

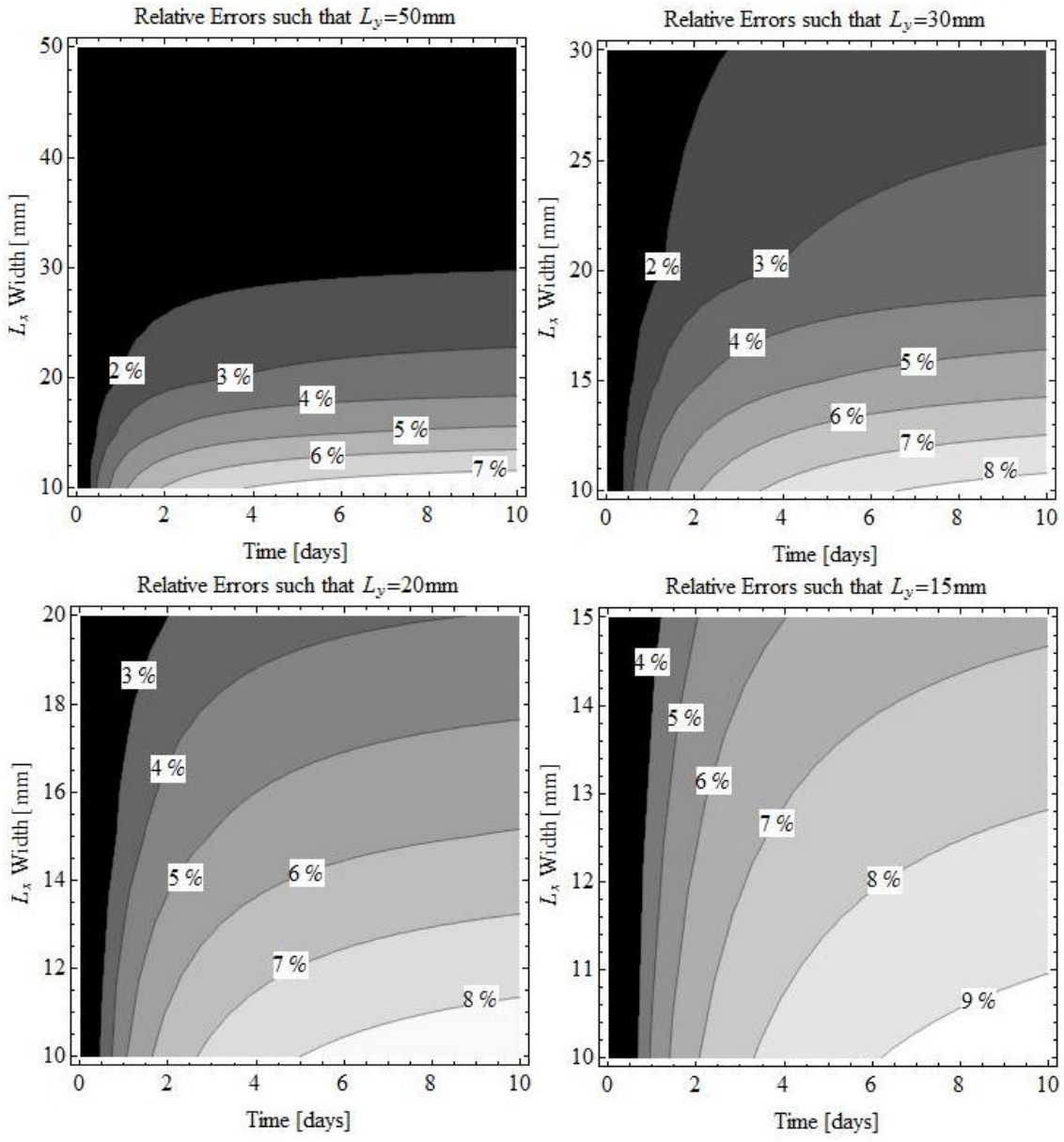

Figure 11-Interpolation of Relative Differences between 2D and 3D Simulations with Variable Domain Sizes; a)L_y=50mm, b) L_y=30mm, c) L_y=20mm, d) L_y=15mm

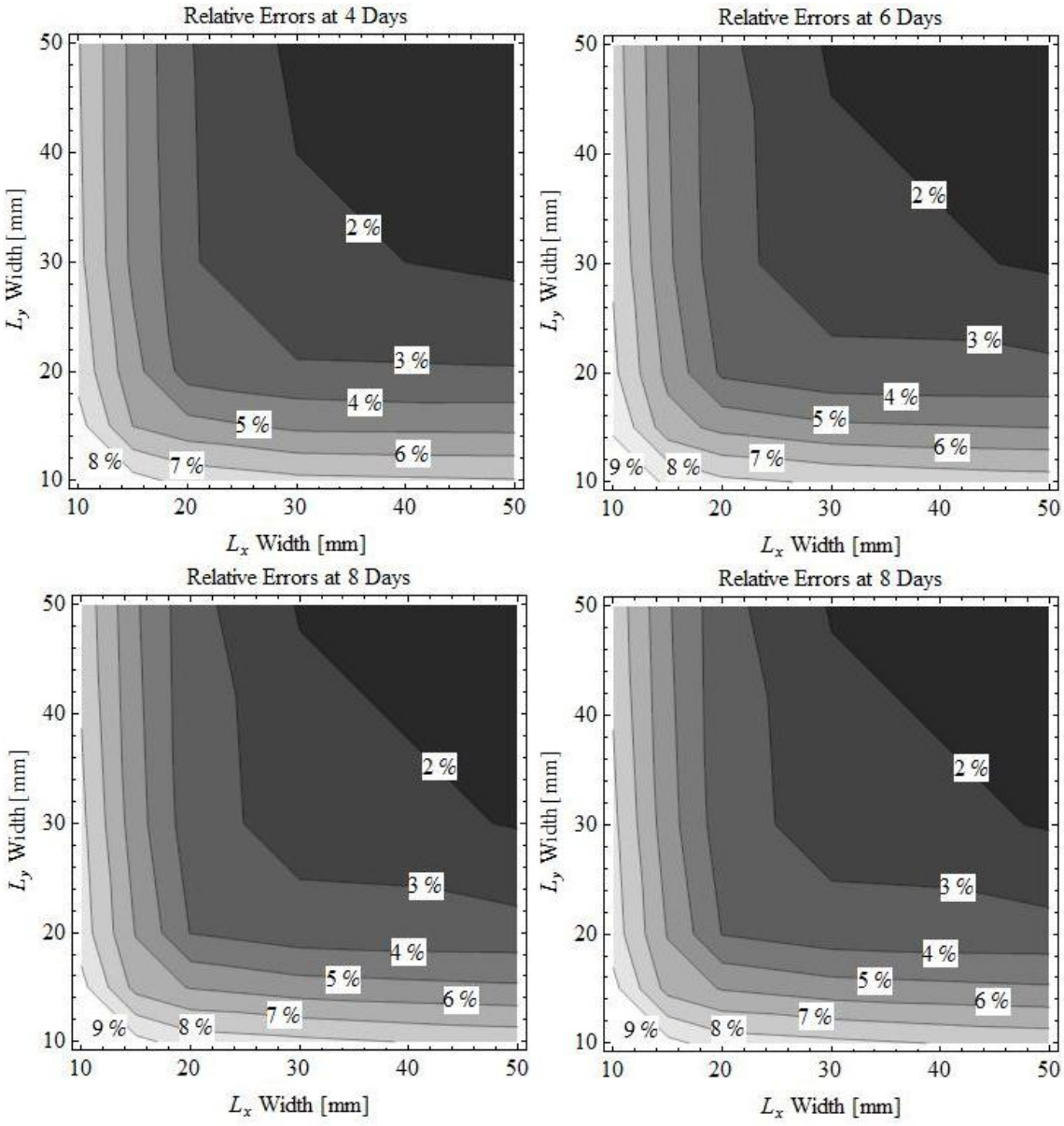

Figure 12-Spatial Error Maps Displaying the Discrepancy in going from 3D to 2D Simulations; a)t=4days, b) t=6days, c) t=8days, d) t=10days

5.3 Comparison of One Dimensional and Three Dimensional Models

Figures 13 and 14 display the growth rate predictions between the 1D and 3D models. Those figures show the effects of changing the size of a square domain for 3D biofilm growth, as well as their relative differences with the 1D model. Figure 15 shows the error map when both the x and y direction lengths are changed at different times.

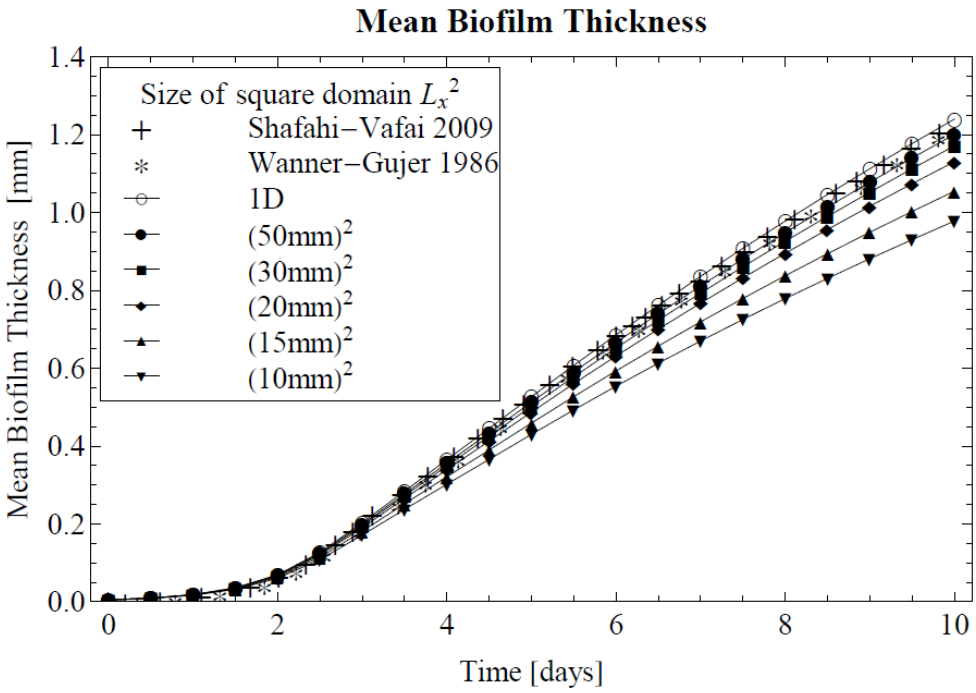

Figure 13-Comparison between 1D and 3D Biofilm Growth with Variable Domain Sizes

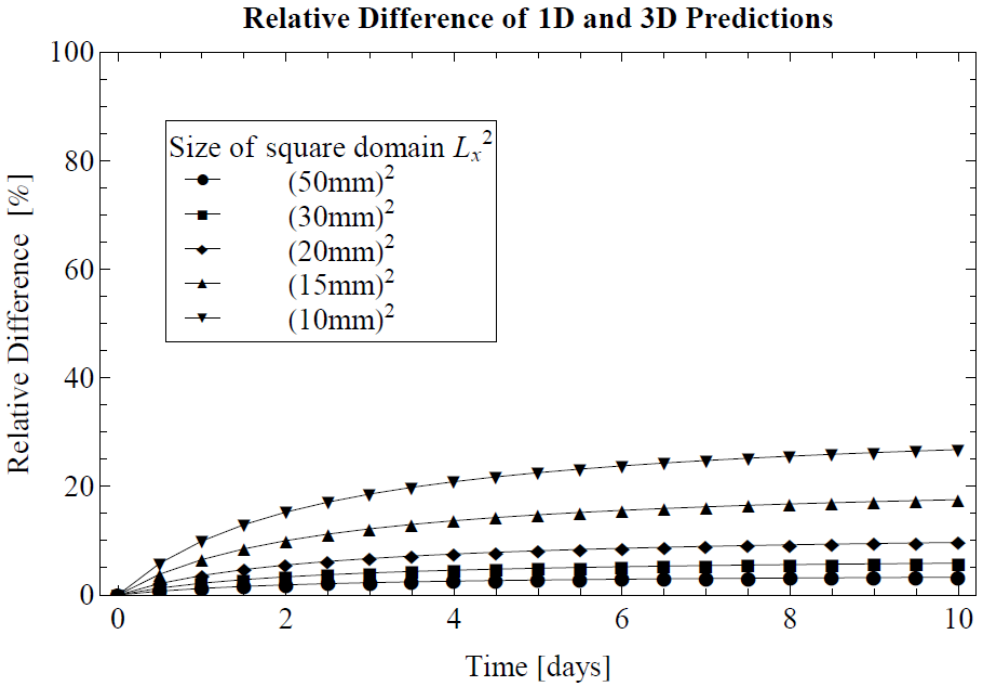

Figure 14-Relative Differences between 1D and 3D Simulations with Variable Domain Sizes

The error maps show that the one dimensional and three dimensional predictions begin to diverge significantly at domain widths of around 20mm. For domain widths greater than 20mm, the one dimensional model predictions provide relatively similar predictions as the three dimensional models.

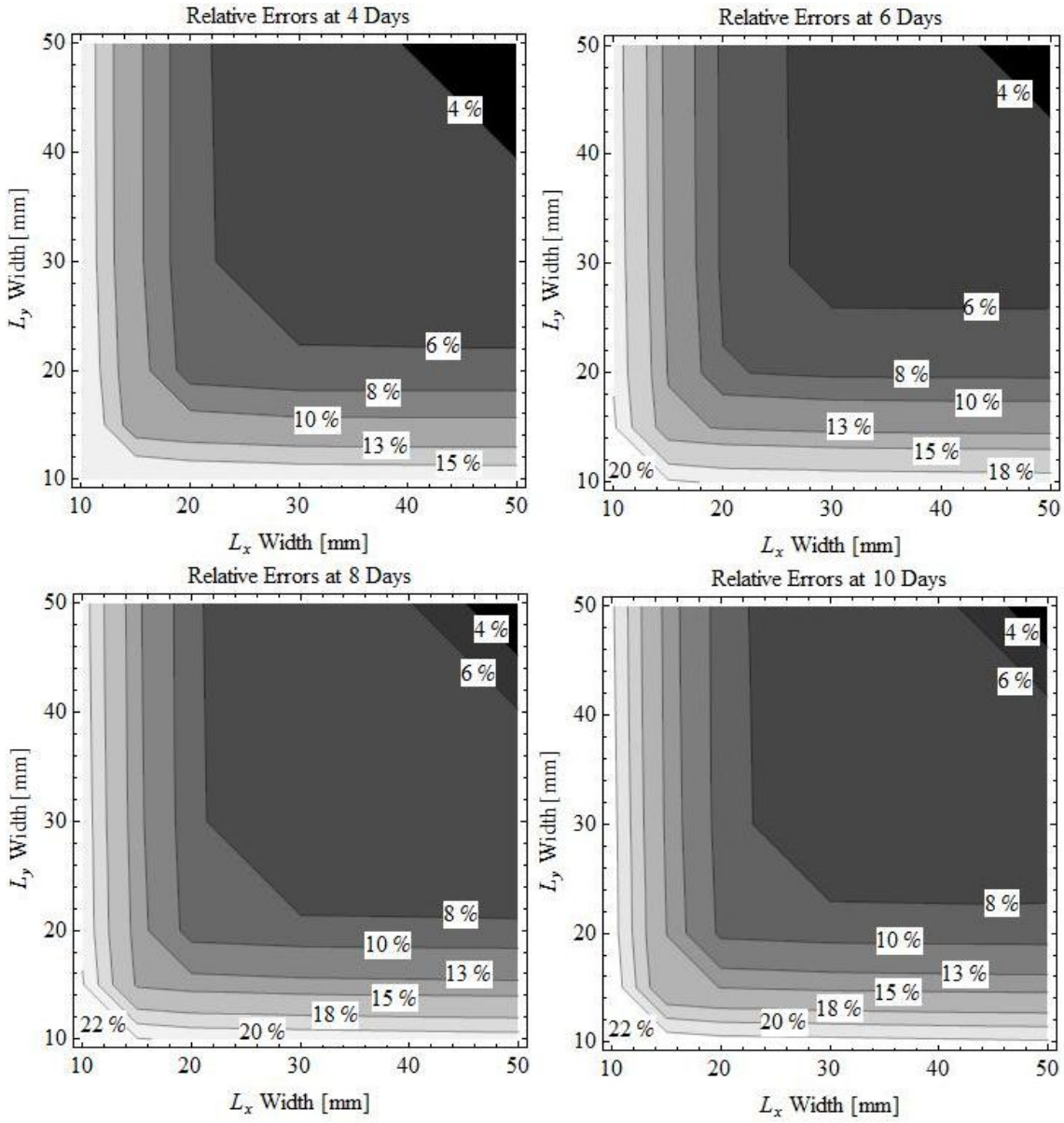

Figure 15-Spatial Error Maps Displaying the Discrepancy in going from 3D to 1D Simulations; a)t=4days, b)t=6days, c)t=8days, d)t=10days

5.4 Comparison of One, Two and Three Dimensional Models applied to the Changing Permeability of a Packed Porous Bed

Using the two species biofilm model composed of bacterial species *Pseudomonas aeruginosa* and EPS, the multidimensional models are applied to investigate the changing permeability of a porous medium composed of a heterogeneously packed bed of spheres [22]. Details of the porous media model, and its various geometrical attributes, are given in Shafahi-Vafai [8].

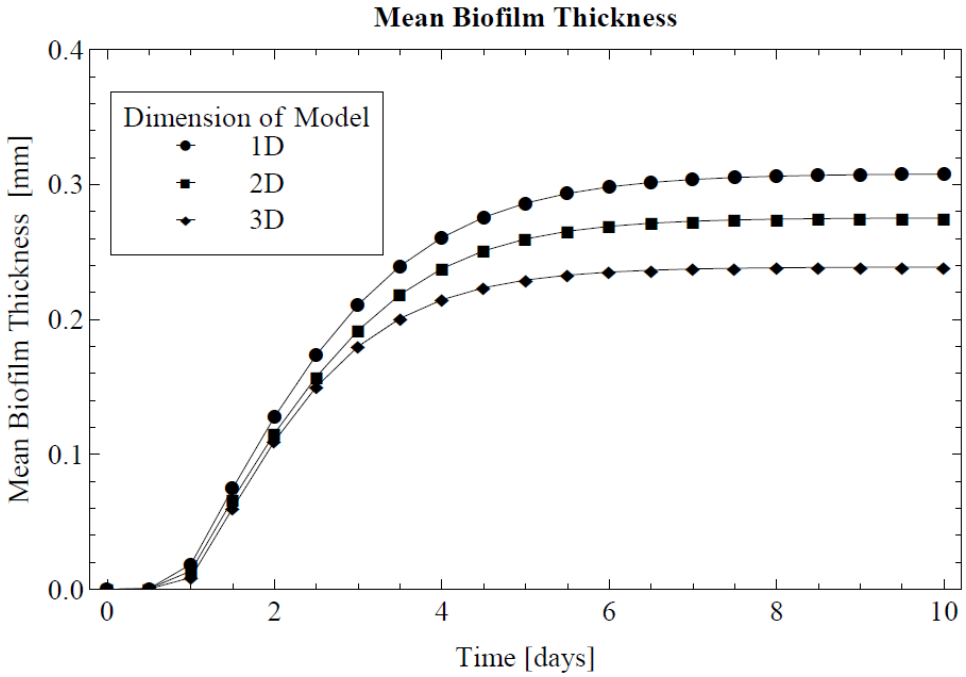

Figure 16-Multidimensional Effect on the Mean Thickness of 2-Species Biofilm with Shearing

The results for the biofilm growth and permeability ratio reduction are given in Figs. 16 and 17. As noted before, the three species model has a slower growth rate in higher dimensional models. This is also the case when a two species model is considered. This leads to a slightly lower rate of decrease of the permeability of the porous bed for higher

dimensional models. It is established that the one dimensional model is in very good agreement with its two and three dimensional analogues.

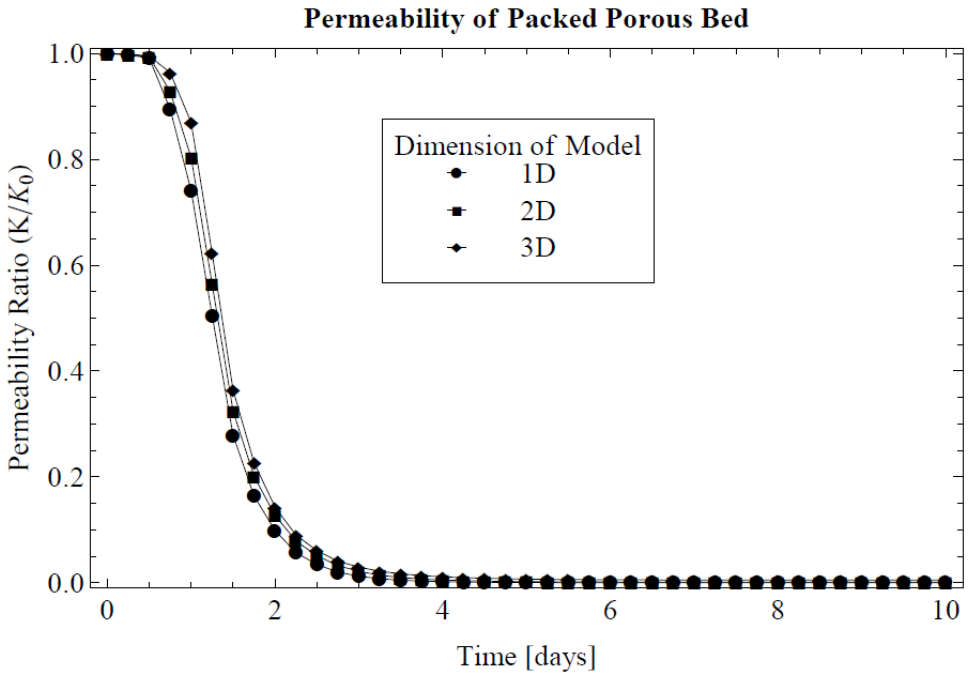

Figure 17-Multidimensional Effect on the Permeability of a Porous Bed

CHAPTER 6

Conclusions

A general multidimensional, multispecies, heterogeneous continuum biofilm model was developed. Two general case studies were analyzed for multidimensional effects, the first being a 3-species system composed of heterotrophic bacteria, autotrophic bacteria and EPS, and the second being a 2-species system composed of the bacteria *Pseudomonas aeruginosa* and EPS. For the 3-species system, error maps were developed giving the relative differences of the one, two and three dimensional model predictions. For the 2-species system, the biofilm model was applied to a porous media model defined by a packed bed of spheres, and the changes in permeability were predicted and analyzed. In general, the range and validity of the one dimensional models was established and was found to cover a wide range of applications.

REFERENCES

[1] A. D. Higgins, M. E. Pomianek, C. M. Kraml, R. K. Taylor, M. F. Semmelhack and B. L. Bassler, "The major Vibrio cholerae autoinducer and its role in virulence factor production," *Nature,* vol. 450, no. 7171, pp. 883-886, 2007.

[2] J. W. Costerton, P. S. Stewart and E. P. Greenberg, "Bacterial biofilms: A common cause of persistent infections," *Science,* vol. 284, no. 5418, pp. 1318-1322, 1999.

[3] J. Wanner, K. Kucman and P. Grau, "Activated-Sludge Process Combined with Biofilm Cultivation," *Water Research,* vol. 22, no. 2, pp. 207-215, 1988.

[4] C. M. Waters and B. L. Bassler, "Quorum Sensing: Cell-to-Cell Communication in Bacteria," *The Annual Review of Cell and Developmental Biology,* vol. 21, pp. 319-346, 2005.

[5] W. Gujer and O. Wanner, "A Multispecies Biofilm Model," *Biotechnology and Bioengineering,* vol. XXVIII, 1986.

[6] E. Alpkvist and I. Klapper, "A Multidimensional multispecies continuum model for heterogeneous biofilm development," *Bulletin of Mathematica Biology,* pp. 765-789, 2007.

[7] J. Dockery and I. Klapper, "Finger Formation in Biofilm Layers," *Society for Industrial and Applied Mathematics,* vol. 62, no. 3, pp. 853-869, 2001.

[8] M. Shafahi and K. Vafai, "Biofilm affected characteristics of porous structures," *International Journal of Heat and Mass Transfer,* vol. 52, no. 3-4, pp. 574-581, 2009.

[9] M. Shafahi and K. Vafai, "Synthesis of biofilm resistance characteristics against antibiotics," *International Journal of Heat and Mass Transfer,* vol. 53, pp. 2943-2950, 2010.

[10] C. Picioreanu, J.-U. Kreft and M. C. M. van Loosdrecht, "Particle-Based Multidimensional Multispecies Biofilm Model," *Applied and Environmental Microbiology,* vol. 70, no. 5, pp. 3024-3040, 2004.

[11] J.-U. Kreft, C. Picioreanu, J. W. Wimpenny and M. C. van Loosdrecht, "Individual-based modeling of biofilms," *Microbiology,* vol. 147, no. 11, pp. 2897-2912, 2001.

[12] J. U. Kreft and J. W. Wimpenny, "Effect of EPS on biofilm structure and function as revealed by an indivdual-based model of biofilm growth.," *Water Science and*

Technology, vol. 43, no. 6, pp. 135-141, 2001.

[13] S. W. Hermanowicz, "A simple 2D biofilm model yields a variety of morphological features," *Mathematical Biosciences,* vol. 169, no. 1, pp. 1-14, 2001.

[14] J. W. Wimpenny and R. Colasanti, "A unifying hypothesis for the structure of microbial biofilms based on cellular automaton models," *FEMS Microbiology Ecology,* vol. 22, no. 1, pp. 1-16, 1997.

[15] C. Picioreanu, M. C. van Loosdrecht and J. J. Heijnen, "Mathematical modeling of biofilm structure with a hybrid differential-discrete cellular automaton approach," *Biotechnology and Bioengineering,* vol. 58, no. 1, pp. 101-116, 2000.

[16] E. Alpkvist, C. Picioreanu, M. C. van Loosdrecht and A. Heyden, "Three-Dimensional Biofilm Model With Individual Cells and Continuum EPS Matrix," *Biotechnology and Bioengineering,* vol. 94, no. 5, 2006.

[17] B. E. Rittmann and P. L. McCarty, "Model of Steady-State-Biofilm Kinetics," *Biotechnology and Bioengineering,* vol. XXII, pp. 2343-2357, 1980.

[18] B. E. Rittmann and J. A. Manem, "Development and Experimental Evaluation of a Steady-State, Multispecies Biofilm Model," *Biotechnology and Bioengineering,* vol. 39, no. 9, 1991.

[19] C. Picioreanu, M. C. van Loosdrecht and J. J. Heijnen, "Discrete-differential modelling of biofilm-structure," *Water Science and Technology,* vol. 39, no. 7, pp. 115-122, 1999.

[20] J. A. Sethian, Level Set Methods and Fast Marching Methods, Cambridge: Cambridge University Press, 1999.

[21] O. Wanner, A. B. Cunningham and R. Lundman, "Modeling Biofilm Accumulation and Mass Transport in a Porous Medium Under High Substrate Loading," *Biotechnology and Bioengineering,* vol. 47, no. 6, pp. 703-712, 1995.

[22] S. W. Taylor, P. Milly and P. R. Jaffe, "Biofilm Growth and the Related Changes in the Physical Properties of a Porous Medium 2. Permeability," *Water Resources Research,* vol. 26, no. 9, pp. 2161-2169, 1990.

[23] A. D. Higgins, M. E. Pomianek, C. M. Kraml, R. K. Taylor, M. F. Semmelhack and B. L. Bassler, "The major Vibrio cholerae autoinducer and its role in virulence factor production," *Nature,* vol. 450, no. 7171, pp. 883-886, 2007.

[24] J. W. Costerton, P. S. Stewart and E. P. Greenberg, "Bacterial biofilms: A common cause of persistent infections," *Science,* vol. 284, no. 5418, pp. 1318-1322, 1999.

[25] J. Wanner, K. Kucman and P. Grau, "Activated-Sludge Process Combined with Biofilm Cultivation," *Water Research,* vol. 22, no. 2, pp. 207-215, 1988.

APPENDIX A

Using differential operators (18)-(21), (23), fourth-order accurate finite differencing approximations will be applied to the governing equations (24)-(27). The derivations of the finite difference equations are shown here.

A.1 Surface tracking equation:

The surface tracking equation is written in the compact form:

$$\vec{S} = \vec{S}_0 - \int_0^t \vec{\nabla}\Phi dt \tag{38}$$

This can be written explicitly as:

$$\vec{S} = \langle x, y, Z_0 \rangle - \int_0^t \left\langle \frac{\partial \Phi}{\partial x}, \frac{\partial \Phi}{\partial y}, \frac{\partial \Phi}{\partial z} \right\rangle dt \tag{39}$$

In the new coordinate space, (39) becomes (note that z'=1 at the surface):

$$\vec{S} = \langle L_x x', L_y y', Z_0 \rangle$$
$$-\int_0^t \left\langle \frac{1}{L_x}\frac{\partial \Phi}{\partial x'} - \frac{1}{L_x}\frac{\partial_{x'} Z}{Z}\frac{\partial \Phi}{\partial z'}, \frac{1}{L_y}\frac{\partial \Phi}{\partial y'} - \frac{1}{L_y}\frac{\partial_{y'} Z}{Z}\frac{\partial \Phi}{\partial z'}, \frac{1}{Z}\frac{\partial \Phi}{\partial z'} \right\rangle dt \tag{40}$$

Apply finite differencing to this equation:

$$\vec{S}_{i,j}^{n+1} = \left(\begin{array}{l} L_x (i-1)\Delta x' + \dfrac{\Delta t}{2\Delta x' L_x}\left(\Phi^n_{i+1,j,\mathrm{kmax}} - \Phi^n_{i-1,j,\mathrm{kmax}}\right) \\ -\dfrac{\Delta t}{4\Delta x'\Delta z' L_x Z^n_{i,j}}\left(Z^n_{i+1,j} - Z^n_{i-1,j}\right)\left(\Phi^n_{i,j,\mathrm{kmax}-2} - 4\Phi^n_{i,j,\mathrm{kmax}-1} + 3\Phi^n_{i,j,\mathrm{kmax}}\right) \end{array} \right)\hat{x}$$
$$+ \left(\begin{array}{l} L_y (j-1)\Delta y' + \dfrac{\Delta t}{2\Delta y' L_y}\left(\Phi^n_{i,j+1,\mathrm{kmax}} - \Phi^n_{i,j-1,\mathrm{kmax}}\right) \\ -\dfrac{\Delta t}{4\Delta y'\Delta z' L_y Z^n_{i,j}}\left(Z^n_{i,j+1} - Z^n_{i,j-1}\right)\left(\Phi^n_{i,j,\mathrm{kmax}-2} - 4\Phi^n_{i,j,\mathrm{kmax}-1} + 3\Phi^n_{i,j,\mathrm{kmax}}\right) \end{array} \right)\hat{y} \qquad (41)$$
$$+ \left(Z^n_{i,j} - \frac{\Delta t}{2\Delta z' Z^n_{i,j}}\left(\Phi^n_{i,j,\mathrm{kmax}-2} - 4\Phi^n_{i,j,\mathrm{kmax}-1} + 3\Phi^n_{i,j,\mathrm{kmax}}\right)\right)\hat{z}$$

A.2 Growth equation:

The growth equation is written in the compact form:

$$\frac{\partial v_s}{\partial t} - \vec{\nabla}\Phi \cdot \vec{\nabla} v_s = \frac{g_s}{\rho_s^*} - v_s \sum_i \frac{g_i}{\rho_i^*} \qquad (42)$$

This expands to the following:

$$\frac{\partial v_s}{\partial t} - \frac{\partial \Phi}{\partial x}\cdot\frac{\partial v_s}{\partial x} - \frac{\partial \Phi}{\partial y}\cdot\frac{\partial v_s}{\partial y} - \frac{\partial \Phi}{\partial z}\cdot\frac{\partial v_s}{\partial z} = \frac{g_s}{\rho_s^*} - v_s \sum_i \frac{g_i}{\rho_i^*} \qquad (43)$$

Apply the new differential operators:

$$\left(\frac{1}{\tau}\frac{\partial v_s}{\partial t'} - \frac{z'}{\tau}\frac{\partial_{t'} Z}{Z}\frac{\partial v_s}{\partial z'}\right) - \left(\frac{1}{L_x}\frac{\partial \Phi}{\partial x'} - \frac{z'}{L_x}\frac{\partial_{x'} Z}{Z}\frac{\partial \Phi}{\partial z'}\right)\cdot\left(\frac{1}{L_x}\frac{\partial v_s}{\partial x'} - \frac{z'}{L_x}\frac{\partial_{x'} Z}{Z}\frac{\partial v_s}{\partial z'}\right) -$$
$$-\left(\frac{1}{L_y}\frac{\partial \Phi}{\partial y'} - \frac{z'}{L_y}\frac{\partial_{y'} Z}{Z}\frac{\partial \Phi}{\partial z'}\right)\cdot\left(\frac{1}{L_y}\frac{\partial v_s}{\partial y'} - \frac{z'}{L_y}\frac{\partial_{y'} Z}{Z}\frac{\partial v_s}{\partial z'}\right) - \left(\frac{1}{Z}\frac{\partial \Phi}{\partial z'}\right)\cdot\left(\frac{1}{Z}\frac{\partial v_s}{\partial z'}\right)$$
$$= \frac{g_s}{\rho_s^*} - v_s \sum_i \frac{g_i}{\rho_i^*} \qquad (44)$$

Simplify:

$$\frac{1}{\tau}\frac{\partial v_s}{\partial t'} = \frac{g_s}{\rho_s^*} - v_s\sum_i \frac{g_i}{\rho_i^*} + \frac{\partial v_s}{\partial x'}\frac{1}{L_x{}^2}\left(\frac{\partial \Phi}{\partial x'} - z'\frac{\partial_{x'}Z}{Z}\frac{\partial \Phi}{\partial z'}\right) + \frac{\partial v_s}{\partial y'}\frac{1}{L_y{}^2}\left(\frac{\partial \Phi}{\partial y'} - z'\frac{\partial_{y'}Z}{Z}\frac{\partial \Phi}{\partial z'}\right) +$$
$$\frac{\partial v_s}{\partial z'}\left(\frac{z'}{\tau}\frac{\partial_{t'}Z}{Z} - \frac{1}{L_x{}^2}\left(\frac{\partial \Phi}{\partial x'} - z'\frac{\partial_{x'}Z}{Z}\frac{\partial \Phi}{\partial z'}\right)z'\frac{\partial_{x'}Z}{Z} - \frac{1}{L_y{}^2}\left(\frac{\partial \Phi}{\partial y'} - z'\frac{\partial_{y'}Z}{Z}\frac{\partial \Phi}{\partial z'}\right)z'\frac{\partial_{y'}Z}{Z} + \frac{1}{Z^2}\left(\frac{\partial \Phi}{\partial z'}\right)\right)$$

(45)

Apply finite differencing approximations by discretizing the differential equation:

$$\frac{1}{\tau}\frac{v_{i,j,k}^{n+1} - v_{i,j,k}^{n}}{\Delta t'} = \frac{g_s}{\rho_s^*} - v_s\sum_i \frac{g_i}{\rho_i^*}$$
$$+ \frac{v_{i+1,j,k}^{n} - v_{i-1,j,k}^{n}}{2\Delta x'}\frac{1}{L_x{}^2}\left(\frac{\Phi_{i+1,j,k}^{n} - \Phi_{i-1,j,k}^{n}}{2\Delta x'} - \frac{z'}{Z}\frac{Z_{i+1,j,k}^{n} - Z_{i-1,j,k}^{n}}{2\Delta x'}\frac{\Phi_{i,j,k+1}^{n} - \Phi_{i,j,k-1}^{n}}{2\Delta z'}\right)$$
$$+ \frac{v_{i,j+1,k}^{n} - v_{i,j-1,k}^{n}}{2\Delta y'}\frac{1}{L_y{}^2}\left(\frac{\Phi_{i,j+1,k}^{n} - \Phi_{i,j-1,k}^{n}}{2\Delta y'} - \frac{z'}{Z}\frac{Z_{i,j+1,k}^{n} - Z_{i,j-1,k}^{n}}{2\Delta y'}\frac{\Phi_{i,j,k+1}^{n} - \Phi_{i,j,k-1}^{n}}{2\Delta z'}\right)$$
$$+ \frac{v_{i,j,k+1}^{n} - v_{i,j,k-1}^{n}}{2\Delta z'}\left(\begin{array}{l}\frac{z'}{\tau Z}\frac{Z_{i,j,k}^{n+1} - Z_{i,j,k}^{n-1}}{2\Delta t'} \\ -\frac{1}{L_x{}^2}\left(\begin{array}{l}\frac{\Phi_{i+1,j,k}^{n} - \Phi_{i-1,j,k}^{n}}{2\Delta x'} \\ -\frac{z'}{Z}\frac{Z_{i+1,j,k}^{n} - Z_{i-1,j,k}^{n}}{2\Delta x'}\frac{\Phi_{i,j,k+1}^{n} - \Phi_{i,j,k-1}^{n}}{2\Delta z'}\end{array}\right)\frac{z'}{Z}\frac{Z_{i+1,j,k}^{n} - Z_{i-1,j,k}^{n}}{2\Delta x'} \\ -\frac{1}{L_y{}^2}\left(\begin{array}{l}\frac{\Phi_{i,j+1,k}^{n} - \Phi_{i,j-1,k}^{n}}{2\Delta y'} \\ -\frac{z'}{Z}\frac{Z_{i,j+1,k}^{n} - Z_{i,j-1,k}^{n}}{2\Delta y'}\frac{\Phi_{i,j,k+1}^{n} - \Phi_{i,j,k-1}^{n}}{2\Delta z'}\end{array}\right)\frac{z'}{Z}\frac{Z_{i,j+1,k}^{n} - Z_{i,j-1,k}^{n}}{2\Delta y'} \\ +\frac{1}{Z^2}\frac{\Phi_{i,j,k+1}^{n} - \Phi_{i,j,k-1}^{n}}{2\Delta z'}\end{array}\right)$$

(46)

From this equation, one can explicitly solve for the advanced time step volume fraction:

$$
\begin{aligned}
v_{i,j,k}^{n+1} &= v_{i,j,k}^{n} + \tau\Delta t' \left(\frac{g_s}{\rho_s^*} - v_s \sum_i \frac{g_i}{\rho_i^*} \right) \\
&+ \left(v_{i+1,j,k}^{n} - v_{i-1,j,k}^{n} \right) \frac{\tau\Delta t}{\left(2\Delta x'\right)^2 L_x^{\,2}} \left(\begin{array}{l} \left(\Phi_{i+1,j,k}^{n} - \Phi_{i-1,j,k}^{n} \right) \\ -\dfrac{z'}{2\Delta z' Z} \left(Z_{i+1,j,k}^{n} - Z_{i-1,j,k}^{n} \right) \left(\Phi_{i,j,k+1}^{n} - \Phi_{i,j,k-1}^{n} \right) \end{array} \right) \\
&+ \left(v_{i,j+1,k}^{n} - v_{i,j-1,k}^{n} \right) \frac{\tau\Delta t}{\left(2\Delta y'\right)^2 L_y^{\,2}} \left(\begin{array}{l} \left(\Phi_{i,j+1,k}^{n} - \Phi_{i,j-1,k}^{n} \right) \\ -\dfrac{z'}{2\Delta z' Z} \left(Z_{i,j+1,k}^{n} - Z_{i,j-1,k}^{n} \right) \left(\Phi_{i,j,k+1}^{n} - \Phi_{i,j,k-1}^{n} \right) \end{array} \right) \\
&+ \left(v_{i,j,k+1}^{n} - v_{i,j,k-1}^{n} \right) \frac{\tau\Delta t'}{2\Delta z'} \left(\begin{array}{l} \dfrac{z'}{2\Delta t' \tau Z} \left(Z_{i,j,k}^{n+1} - Z_{i,j,k}^{n-1} \right) \\ -\dfrac{1}{\left(2\Delta x'\right)^2 L_x^{\,2}} \dfrac{z'}{Z} \left(\begin{array}{l} \left(\Phi_{i+1,j,k}^{n} - \Phi_{i-1,j,k}^{n} \right) \left(Z_{i+1,j,k}^{n} - Z_{i-1,j,k}^{n} \right) \\ -\dfrac{z'}{2\Delta z' Z} \left(Z_{i+1,j,k}^{n} - Z_{i-1,j,k}^{n} \right)^2 \left(\Phi_{i,j,k+1}^{n} - \Phi_{i,j,k-1}^{n} \right) \end{array} \right) \\ -\dfrac{1}{\left(2\Delta y'\right)^2 L_y^{\,2}} \dfrac{z'}{Z} \left(\begin{array}{l} \left(\Phi_{i,j+1,k}^{n} - \Phi_{i,j-1,k}^{n} \right) \left(Z_{i,j+1,k}^{n} - Z_{i,j-1,k}^{n} \right) \\ -\dfrac{z'}{2\Delta z' Z} \left(Z_{i,j+1,k}^{n} - Z_{i,j-1,k}^{n} \right)^2 \left(\Phi_{i,j,k+1}^{n} - \Phi_{i,j,k-1}^{n} \right) \end{array} \right) \\ +\dfrac{1}{2\Delta z' Z^2} \left(\Phi_{i,j,k+1}^{n} - \Phi_{i,j,k-1}^{n} \right) \end{array} \right)
\end{aligned}
$$

(47)

A.3 Poisson's equation:

Both the nutrient equation and the potential equation are of the form of Poisson's equation:

$$\nabla^2 f = g \tag{48}$$

In the new coordinate space, this may be written as:

$$\begin{aligned}
&\frac{1}{L_x^{\,2}}\frac{\partial^2 f}{\partial x'^2}+\frac{1}{L_y^{\,2}}\frac{\partial^2 f}{\partial y'^2}+\frac{1}{Z^2}\left(1+z'\left(\left(\frac{\partial_{x'}Z}{L_x}\right)^2+\left(\frac{\partial_{y'}Z}{L_y}\right)^2\right)\right)\frac{\partial^2 f}{\partial z'^2}\\
&\quad -2\frac{z'}{L_x^{\,2}}\frac{\partial_{x'}Z}{Z}\frac{\partial^2 f}{\partial x'\partial z'}-2\frac{z'}{L_y^{\,2}}\frac{\partial_{y'}Z}{Z}\frac{\partial^2 f}{\partial y'\partial z'}\\
&\quad +\frac{z'}{Z^2}\left(\frac{2\left(\partial_{x'}Z\right)^2-\left(\partial_{x'}{}^2Z\right)Z}{L_x^{\,2}}+\frac{2\left(\partial_{y'}Z\right)^2-\left(\partial_{y'}{}^2Z\right)Z}{L_y^{\,2}}\right)\frac{\partial f}{\partial z'}=g
\end{aligned} \tag{49}$$

Re-write:

$$\begin{aligned}
&\frac{Z^2}{L_x^{\,2}}\frac{\partial^2 f}{\partial x'^2}+\frac{Z^2}{L_y^{\,2}}\frac{\partial^2 f}{\partial y'^2}+\left(1+z'\left(\left(\frac{\partial_{x'}Z}{L_x}\right)^2+\left(\frac{\partial_{y'}Z}{L_y}\right)^2\right)\right)\frac{\partial^2 f}{\partial z'^2}\\
&\quad -2\frac{z'Z}{L_x^{\,2}}\frac{\partial Z}{\partial x'}\frac{\partial^2 f}{\partial x'\partial z'}-2\frac{z'Z}{L_y^{\,2}}\frac{\partial Z}{\partial y'}\frac{\partial^2 f}{\partial y'\partial z'}\\
&\quad +z'\left(\frac{2\left(\partial_{x'}Z\right)^2-\left(\partial_{x'}{}^2Z\right)Z}{L_x^{\,2}}+\frac{2\left(\partial_{y'}Z\right)^2-\left(\partial_{y'}{}^2Z\right)Z}{L_y^{\,2}}\right)\frac{\partial f}{\partial z'}=Z^2 g
\end{aligned} \tag{50}$$

For brevity, define the following:

$$a=\frac{Z^2}{L_x{}^2},\ b=\frac{Z^2}{L_y{}^2},\ c=\left(1+z'\left(\left(\frac{\partial_{x'}Z}{L_x}\right)^2+\left(\frac{\partial_{y'}Z}{L_y}\right)^2\right)\right)$$

$$d=-2\frac{z'Z}{L_x{}^2}\frac{\partial Z}{\partial x'},\ e=-2\frac{z'Z}{L_y{}^2}\frac{\partial Z}{\partial y'}\frac{\partial^2 f}{\partial y'\partial z'} \tag{51}$$

$$h=z'\left(\frac{2\left(\partial_{x'}Z\right)^2-\left(\partial_{x'}{}^2Z\right)Z}{L_x{}^2}+\frac{2\left(\partial_{y'}Z\right)^2-\left(\partial_{y'}{}^2Z\right)Z}{L_y{}^2}\right)$$

Substitute (51) into (50)

$$a\frac{\partial^2 f}{\partial x'{}^2}+b\frac{\partial^2 f}{\partial y'{}^2}+c\frac{\partial^2 f}{\partial z'{}^2}+d\frac{\partial^2 f}{\partial x'\partial z'}+e\frac{\partial^2 f}{\partial y'\partial z'}+h\frac{\partial f}{\partial z'}=Z^2 g \tag{52}$$

Apply finite differencing approximations to (51):

$$a_{i,j}^{n+1}=\frac{\left(Z_{i,j}^{n+1}\right)^2}{L_x{}^2},\ b_{i,j}^{n+1}=\frac{\left(Z_{i,j}^{n+1}\right)^2}{L_y{}^2},\ c_{i,j}^{n+1}=\left(1+\left(k-1\right)\Delta z'\left(\left(\frac{Z_{i+1,j}^{n+1}-Z_{i-1,j}^{n+1}}{2\Delta x'L_x}\right)^2+\left(\frac{Z_{i,j+1}^{n+1}-Z_{i,j-1}^{n+1}}{2\Delta y'L_y}\right)^2\right)\right)$$

$$d_{i,j}^{n+1}=-2\frac{\left(k-1\right)\Delta z'Z_{i,j}^{n+1}}{L_x{}^2}\frac{Z_{i+1,j}^{n+1}-Z_{i-1,j}^{n+1}}{2\Delta x'},\ e_{i,j}^{n+1}=-2\frac{\left(k-1\right)\Delta z'Z_{i,j}^{n+1}}{L_y{}^2}\frac{Z_{i,j+1}^{n+1}-Z_{i,j-1}^{n+1}}{2\Delta y'}$$

$$h_{i,j}^{n+1}=\left(k-1\right)\Delta z'\left(\begin{array}{l}2\left(\frac{Z_{i+1,j}^{n+1}-Z_{i-1,j}^{n+1}}{2\Delta x'L_x}\right)^2-\left(\frac{Z_{i+1,j}^{n+1}-2Z_{i,j}^{n+1}+Z_{i-1,j}^{n+1}}{\Delta x'{}^2L_x{}^2}\right)Z_{i,j}^{n+1}\\+2\left(\frac{Z_{i,j+1}^{n+1}-Z_{i,j-1}^{n+1}}{2\Delta y'L_y}\right)^2-\left(\frac{Z_{i,j+1}^{n+1}-2Z_{i,j}^{n+1}+Z_{i,j-1}^{n+1}}{\Delta y'{}^2L_y{}^2}\right)Z_{i,j}^{n+1}\end{array}\right) \tag{53}$$

Apply finite differencing approximation to (52):

$$a_{i,j}^{n+1}\frac{f_{i+1,j,k}^{n+1}-2f_{i,j,k}^{n+1}+f_{i-1,j,k}^{n+1}}{\Delta x'{}^2}+b_{i,j}^{n+1}\frac{f_{i,j+1,k}^{n+1}-2f_{i,j,k}^{n+1}+f_{i,j-1,k}^{n+1}}{\Delta y'{}^2}+c_{i,j}^{n+1}\frac{f_{i,j,k+1}^{n+1}-2f_{i,j,k}^{n+1}+f_{i,j,k-1}^{n+1}}{\Delta z'{}^2}$$

$$+d_{i,j}^{n+1}\frac{f_{i+1,j,k+1}^{n+1}-f_{i+1,j,k-1}^{n+1}-f_{i-1,j,k+1}^{n+1}+f_{i-1,j,k-1}^{n+1}}{4\Delta x'\Delta z'}+e_{i,j}^{n+1}\frac{f_{i,j+1,k+1}^{n+1}-f_{i,j+1,k-1}^{n+1}-f_{i,j-1,k+1}^{n+1}+f_{i,j-1,k-1}^{n+1}}{4\Delta y'\Delta z'}$$

$$+h_{i,j}^{n+1}\frac{f_{i,j,k+1}^{n+1}-f_{i,j,k-1}^{n+1}}{2\Delta z'}=\left(Z_{i,j}^{n+1}\right)^2 g_{i,j,k}^{n+1} \tag{54}$$

Factor (54) for function *f*:

$$
\begin{aligned}
&f_{i+1,j,k}^{n+1}\left(a_{i,j}^{n+1}\Delta y'^{2}\,\Delta z'^{2}\right)+f_{i-1,j,k}^{n+1}\left(b_{i,j}^{n+1}\Delta y'^{2}\,\Delta z'^{2}\right)\\
&+f_{i,j+1,k}^{n+1}\left(b_{i,j}^{n+1}\Delta x'^{2}\,\Delta z'^{2}\right)+f_{i,j-1,k}^{n+1}\left(b_{i,j}^{n+1}\Delta x'^{2}\,\Delta z'^{2}\right)\\
&+f_{i,j,k+1}^{n+1}\left(c_{i,j}^{n+1}\Delta x'^{2}\,\Delta y'^{2}+\frac{1}{2}h_{i,j}^{n+1}\Delta x'^{2}\,\Delta y'^{2}\,\Delta z'\right)+f_{i,j,k-1}^{n+1}\left(c_{i,j}^{n+1}\Delta x'^{2}\,\Delta y'^{2}-\frac{1}{2}h_{i,j}^{n+1}\Delta x'^{2}\,\Delta y'^{2}\,\Delta z'\right)\\
&+f_{i,j,k}^{n+1}\left(-2a_{i,j}^{n+1}\Delta y'^{2}\,\Delta z'^{2}-2b_{i,j}^{n+1}\Delta x'^{2}\,\Delta z'^{2}-2c_{i,j}^{n+1}\Delta x'^{2}\,\Delta y'^{2}\right)\\
&+f_{i+1,j,k+1}^{n+1}\left(\frac{1}{4}d_{i,j}^{n+1}\Delta x'\Delta y'^{2}\,\Delta z'\right)+f_{i+1,j,k-1}^{n+1}\left(-\frac{1}{4}d_{i,j}^{n+1}\Delta x'\Delta y'^{2}\,\Delta z'\right)\\
&+f_{i-1,j,k+1}^{n+1}\left(-\frac{1}{4}d_{i,j}^{n+1}\Delta x'\Delta y'^{2}\,\Delta z'\right)+f_{i-1,j,k-1}^{n+1}\left(\frac{1}{4}d_{i,j}^{n+1}\Delta x'\Delta y'^{2}\,\Delta z'\right)\\
&+f_{i,j+1,k+1}^{n+1}\left(\frac{1}{4}e_{i,j}^{n+1}\Delta x'^{2}\,\Delta y'\Delta z'\right)+f_{i,j+1,k-1}^{n+1}\left(-\frac{1}{4}e_{i,j}^{n+1}\Delta x'^{2}\,\Delta y'\Delta z'\right)\\
&+f_{i,j-1,k+1}^{n+1}\left(-\frac{1}{4}e_{i,j}^{n+1}\Delta x'^{2}\,\Delta y'\Delta z'\right)+f_{i,j-1,k-1}^{n+1}\left(\frac{1}{4}e_{i,j}^{n+1}\Delta x'^{2}\,\Delta y'\Delta z'\right)\\
&=\left(\Delta x'\Delta y'\Delta z'Z_{i,j}^{n+1}\right)^{2}g_{i,j,k}^{n+1}
\end{aligned}
\tag{55}
$$

This defines the matrix inversion problem for unknown function *f*.